Available online at www.sciencedirect.com
ScienceDirect
Biosensors and Bioelectronics 22 (2007) 1664–1671
BIOSENSORS & BIOELECTRONICS
www.elsevier.com/locate/bios

Optical forward-scattering for detection of *Listeria monocytogenes* and other *Listeria* species

Padmapriya P. Banada [a], Songling Guo [b], Bulent Bayraktar [c], Euiwon Bae [b], Bartek Rajwa [d,e], J. Paul Robinson [d,e], E. Daniel Hirleman [b], Arun K. Bhunia [a,*]

[a] *Molecular Food Microbiology Laboratory, Department of Food Science, Purdue University, West Lafayette, IN 47907, USA*
[b] *School of Mechanical Engineering, Purdue University, West Lafayette, IN 47907, USA*
[c] *School of Electrical and Computer Engineering, Purdue University, West Lafayette, IN 47907, USA*
[d] *Department of Basic Medical Sciences, Purdue University, West Lafayette, IN 47907, USA*
[e] *Weldon School of Biomedical Engineering, Purdue University, West Lafayette, IN 47907, USA*

Received 3 April 2006; received in revised form 19 June 2006; accepted 24 July 2006
Available online 1 September 2006

Abstract

We demonstrate here the development of a non-invasive optical forward-scattering system, called 'scatterometer' for rapid identification of bacterial colonies. The system is based on the concept that variations in refractive indices and size, relative to the arrangement of cells in bacterial colonies growing on a semi-solid agar surface will generate different forward-scattering patterns. A 1.2–1.5 mm colony size for a 1 mm laser beam and brain heart infusion agar as substrate were used as fixed variables. The current study is focused on exploring identification of *Listeria monocytogenes* and other *Listeria* species exploiting the known differences in their phenotypic characters. Using diffraction theory, we could model the scattering patterns and explain the appearance of radial spokes and the rings seen in the scattering images of *L. monocytogenes*. Further, we have also demonstrated development of a suitable software for the extraction of the features (scalar values) calculated from images of the scattering patterns using Zernike moment invariants and principal component analysis and were grouped using K-means clustering. We achieved 91–100% accuracy in detecting different species. It was also observed that substrate variations affect the scattering patterns of *Listeria*. Finally, a database was constructed based on the scattering patterns from 108 different strains belonging to six species of *Listeria*. The overall system proved to be simple, non-invasive and virtually reagent-less and has the potential for automated user-friendly application for detection and differentiation of *L. monocytogenes* and other *Listeria* species colonies grown on agar plates within 5–10 min analysis time.

Keywords: Light scattering; *Listeria monocytogenes*; Detection; Identification

1. Introduction

Over the past few years there has been increasing interest in non-invasive light-scattering technologies for studying and/or detecting bacterial cells (Fratamico et al., 1998; Kaye, 1998; Perkins and Squirrell, 2000). Light-scattering instruments like surface plasmon resonance (SPR), flow cytometry, etc., have enabled the study of various biological molecules (Leidberg et al., 1983; Shapiro, 2003) and have been a commercial success. Laser spectroscopic techniques for rapid detection of bacterial spores have become very popular non-conventional method (Scully et al., 2002; Hybl et al., 2003).

Polarized differential light scattering as a practical means for characterization of microorganisms has been investigated for bacterial cells in suspension (Wyatt, 1969; Wyatt and Phillips, 1972; Perkins and Squirrell, 2000; Bronk et al., 2001). From the angular variation in the scattered light pattern, information about the bacterial size, shape, internal structure and refractive index, has been determined for identification of *Salmonella typhimurium*, *Escherichia coli* (Salzman et al., 1982) and *Staphylococcus epidermidis* (Stull, 1972). However, there are challenges associated with bacteria in suspension, such as purity of cultures and arrangement of cells (often in chains or clusters). The orientations of and distances between cells change

* Corresponding author. Tel.: +1 765 494 5443; fax: +1 765 494 7953.
E-mail address: bhunia@purdue.edu (A.K. Bhunia).

0956-5663/$ – see front matter © 2006 Elsevier B.V. All rights reserved.
doi:10.1016/j.bios.2006.07.028

with time. However, a colony on a solid surface such as agar is more stable and its optical response could be modeled with scalar diffraction theory.

We used light scattering as a potential non-invasive optical sensor to identify bacterial colonies on agar plates without the need for further sample processing or preparation. A bacterial colony results from an exponential multiplication of a single cell on a nutrient agar surface forming in a characteristic dome-shaped structure. The pattern of scattered light is dependent on the properties of the scatterer including refractive index, size, shape and chemical composition of the colony. The optical back-scattering method is widely used for wafer inspection and for studying biological cells (Hielscher et al., 1997; Kim et al., 2002), but it did not produce reproducible results with bacterial colonies in our investigation (Nebeker et al., 2001). Conversely, optical forward-scattering yielded reproducible scattering patterns with colonies of *E. coli* and also *Listeria* species, and thus was used in further experiments (Guo, 2004).

Since we observed some unique distinguishable features associated with the patterns of *Listeria* spp., we focused our studies primarily on the species belonging to genus *Listeria* and investigated the scatterometer's ability to distinguish them.

The genus *Listeria* is comprised of six species; *L. monocytogenes*, *L. innocua*, *L. welshimeri*, *L. ivanovii*, *L. seeligeri*, and *L. grayi*. They are Gram-positive, rod-shaped, measuring about 0.5–1 μm × 1–2 μm and produce dome-shaped colonies. *L. monocytogenes* is the only member known to be pathogenic to humans, with a high mortality rate in immuno-suppressed populations, and to cause abortion in pregnant women (Vazquez-Boland et al., 2001). *L. ivanovii* is also pathogenic but infects ruminants.

The conventional detection methods based on biochemical, serological or DNA/RNA characterization involves additional steps of sample enrichment in a liquid medium, plating on selective agar media to obtain single colonies, and use of special reagents for DNA isolation and PCR. All these methods take about 3–5 days to get confirmatory results and are labor intensive. PCR-based methods though faster is highly dependent on efficient DNA isolation and also is limited by its accuracy in detecting live bacterial cells, leading to false positive identification (Hitchins, 1998; Jaradat et al., 2002). In recent years, biosensor tools have been used with improved sensitivity but involve multisteps, and some cases these technologies are unable to differentiate live from dead cells (Ivnitski et al., 1999; Bhunia and Lathrop, 2003; Ligler et al., 2003; Geng et al., 2004).

Thus, the major objectives of this study were: (1) to build a scatterometer based on the principle of forward light scattering for bacteria on the solid surface; (2) to investigate the ability of this system to differentiate *Listeria* colonies belonging to different species grown on the surface of agar plates; (3) modeling of the scatter patterns; (4) development of an image analysis tool. Overall, in this paper we propose the development of an efficient, non-invasive, reagent-less, user-friendly biosensing instrumentation with automated image analysis tool for rapid identification of live bacteria.

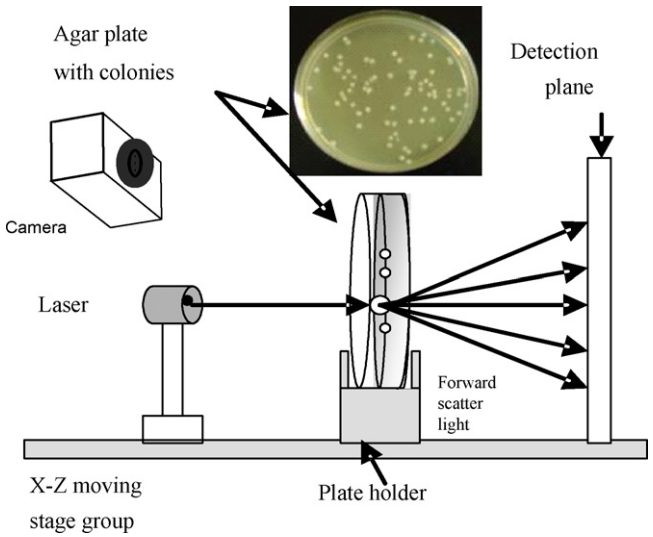

Fig. 1. Schematic drawing of a scatterometer. Inset: photograph of a typical plate (BHI) with *Listeria* colonies.

2. Materials and methods

2.1. Bacterial cultures

The bacterial cultures (108) used in this study are listed in Table 1 (see Supplementary material). They were grown in brain heart infusion (BHI; Difco, Sparks, MD) broth for 18–24 h at 37 °C for subsequent plating on BHI agar plates. Identity of the cultures was confirmed by ribotyping using an automated Riboprinter® (Qualicon, Willmington, DE). *L. monocytogenes* ATCC 23074 transformed with pNF8, a GFP-encoding plasmid was obtained from Dr. B.M. Applegate, Purdue University, for confocal microscopy.

2.2. Preparation of bacterial plates for light-scattering experiments

The culture dilutions were plated on the surface of BHI agar plate (100 mm × 15 mm), so as to obtain 20–30 colonies per plate and were incubated at 37 °C for 24–36 h or until the diameter of the colony reached approximately 1–1.5 mm (Fig. 1, inset). Since the growth rate is different for different species, the size was used as a fixed parameter. The thickness of the colony (along the optical axis), was typically around 0.1–0.3 cm as measured from the surface profile data obtained by laser triangulation probe (Microtrak II Laser Displacement Sensor System, MTI instruments Inc., Albany, NY). A total of 2149 scatter images were acquired from 108 different strains belonging to six species of *Listeria*. On an average of 20 images were obtained per strain, from the colonies growing in two or three different plates.

2.3. Scatterometer

The scatterometer system was built on an optical breadboard for precise and stable positioning of the optical components (Fig. 1) and to provide vibration free base. The system included: a laser diode of 635-nm wavelength; a Petri-plate holder; a detec-

tion plane; a digital camera to acquire the scattering images. The laser, the Petri-plate holder, and the detection plane were placed sequentially on the optical path (*Y*-axis) of the laser beam. The distance from the Petri-plate holder to the laser was 100 mm, and to the detection plane was 300 mm. The laser generates a collimated beam on the order of 1 mm diameter (at the $1/e^2$ irradiance points) that is directed through the center of the bacterial colony and through the substrate of bacterial agar medium. While a fraction of the laser beam was fully transmitted through the substrate and bacterial colony, another fraction was scattered in the forward direction (at relatively small angles to the transmitted beam). The forward-scattered and transmitted light formed the scattering patterns of the bacterial colonies on the detection plane (8 in. × 10 in. white board) and was captured with a digital camera.

2.4. Microscopy

L. monocytogenes ATCC 23074 pNF8, a GFP-expressing strain was used for confocal microscopy. The culture was grown on BHI agar containing 50 μg ml^{-1} erythromycin until the colony size was about 0.2 mm. A confocal microscopic (MRC1024, Bio-Rad) image of a whole single colony of GFP-expressing *L. monocytogenes* excited at 488 nm was taken at 10× and analyzed using the confocal assistant (Version 4.02).

Cryo-scanning electron microscopy for the intact colonies of *L. monocytogenes* ATCC 19113 and *L. innocua* F4248 was carried out to understand the arrangement of the cells in a colony. For the methods and the pictures please see Supplementary material.

2.5. Modeling of scattering patterns using diffraction theory

The confocal microscopic images were used to develop an understanding of the microstructure of the colonies. This allowed diffraction theory to be applied to compute the scattering pattern of GFP-*L. monocytogenes* and simulate unique features such as the rings and radial spokes. Based on the optical theory, the diffraction pattern in the image plane is the Fourier transform of the object plane (Fig. 2) as

$$U(P_0) = \frac{1}{\mathrm{i}\lambda}\int_{\Sigma}\int U(P_1)\frac{\exp(\mathrm{i}kr_{01})}{r_{01}}\cos\theta\,\mathrm{d}s \tag{1}$$

where P_1 denotes a point on the object plane, P_0 a point on the image plane, r_{01} the distance from the object to image plane, λ the wavelength, k the wavenumber, z the distance from the object plane to the image plane, and θ is the angle between r_{01} and z. We approximated the above equation based on diffraction theory and validity criteria (Goodman, 1996; Warner and Hirleman, 1997) as

$$U(x,y) = \frac{\mathrm{e}^{\mathrm{i}kz}}{\mathrm{i}\lambda z}\mathrm{e}^{\mathrm{j}(k/2z)(x^2+y^2)}\int_{\Sigma}\int U'(\xi,\eta)\,\mathrm{e}^{\mathrm{i}(k/2z)(\xi^2+\eta^2)} \times \mathrm{e}^{-\mathrm{i}(2\pi/\lambda z)(x\xi+y\eta)}\,\mathrm{d}\xi\,\mathrm{d}\eta \tag{2}$$

The bottom of the Petri-plate was considered as the object plane for this purpose (Fig. 2). When an incident beam passes through a series of physical objects, the wave front modification was obtained by multiplying the amplitude and phase modulation caused by each independent object.

2.6. Image analysis by Zernike moment features

It was clear from the typical images of *Listeria* that, owing to the circular shapes of the bacterial scattering patterns, the use of Zernike moment invariants, which are unique tools to capture information on circular patterns, was a good choice for feature-extraction and differentiation of species. Therefore, the high-resolution original images were initially downsized to 300-by-300 and the circular scattering patterns were centered in the middle. After performing adaptive histogram equalization (*adapthisteq* function in Matlab®) on the downsized images, Zernike moment invariants of up to 20th order were calculated from them (a total of 120 features). Zernike moments are represented by a set of complex polynomials, which form a complete orthogonal set over the interior of a circle (i.e., $x^2+y^2=1$):

$$V_{nm}(x,y) = V_{nm}(r,\theta) = R_{nm}(r)\,\mathrm{e}^{\mathrm{j}m\theta} \tag{3}$$

where r is the length of a vector from the origin to an (x, y) pixel, θ the angle between vector r and the x-axis in the counterclockwise direction, n a non-negative integer, $|m|$ is less than or equal to n subject to the constraint of $n-|m|$ being an even number, and

$$R_{nm}(r) = \sum_{s=0}^{(n-|m|)/2}\frac{(-1)^s(n-s)!}{s!(((n+|m|)/2)-s)!}r^{n-2s} \times (((n-|m|)/2)-s)! \tag{4}$$

$R_{nm}(r)$ is the radial polynomial.

A Zernike moment (Khotanzad and Hong, 1990; Liao and Pawlak, 1998; Mukundan et al., 2001; Mukundan, 2004) of order

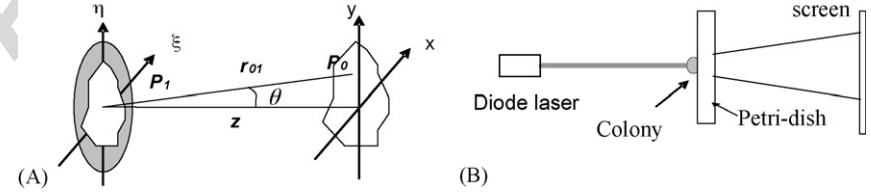

Fig. 2. (A) Coordinates for object plane and image plane and (B) Gaussian beam incident on types of region η and ξ: object planes; P_1: point on the object plane; P_0: object on the image plane; r_{01}: distance from the object to the image plane; z: distance from the object plane to the image plane; θ: angle between r_0 and z; x and y: coordinates for the image plane.

n with repetition m for a digital image function $f(x, y)$ that vanishes outside the unit circle is defined by (asterisk "*" indicates conjugate of a complex number):

$$Z_{nm} = \frac{n+1}{\pi} \sum_x \sum_y f(x, y) V^*_{nm}(r, \theta)\, dx\, dy, \quad x^2 + y^2 \leq 1 \tag{5}$$

Under rotation, the orientation angle of a Zernike moment changes but its magnitude remains unchanged. Therefore, the magnitudes of Zernike moments $|Z_{nm}|$ can be used as rotation-invariant features. To compute the Zernike moments of a given image, the center of the image is taken as the origin and pixel coordinates are mapped to the range of the unit circle. Those pixels falling outside the unit circle are not used.

Our analysis consisted of using PCA as a dimensionality reduction tool on the Zernike moment invariant features and also as an initial grouping of the data. K-means clustering was then used to reach the final classification rate. Image pre-processing, Zernike moment invariants, and K-means clustering were all performed using the Matlab® software (The MathWorks Inc., Natick, MA). Principal component analysis was done using CytoSpec™ (developed by Valeri Patsekin, Cytometry Labs, Purdue University).

2.7. Effect of different agar media on Listeria scattering patterns

L. monocytogenes ATCC 19113 was chosen for growth on different substrates. Nutrient media included brain heart infusion agar (BHIA; Difco); tryptic soy agar (TSA; Difco) and selective (with antimicrobial agents) agar media: *Listeria* repair agar (LRA); buffered *Listeria* enrichment agar (BLEA); polymyxin B–acriflavin–lithium chloride–ceftazidime–aesculin–mannitol (PALCAM) agar. PALCAM contains aesculin (the sugar component reducing to black pigment) to differentiate bacterial colonies. We prepared this medium by omitting aesculin which may otherwise affect the scattering. The antimicrobial supplements acriflavin, cyclohexamide and nalidixic acid were added to each medium as recommended by the US Food and Drug Administration (FDA) (Hitchins, 1998). Scattering patterns obtained for colonies from different media were then grouped using the developed software.

3. Results

3.1. Optical forward-scattering analysis of Listeria colonies on agar plate

The representative scattering patterns of *L. monocytogenes* ATCC 19113, *L. ivanovii* ATCC19119, *L. innocua* F4248, *L. seeligeri* LA15, *L. welshimeri* ATCC 35897 and *L. grayi* Lm37 are shown in Fig. 3. A total of 17 different strains of *L. innocua*, 12 of *L. ivanovii*, 5 of *L. seeligeri*, 3 of *L. welshimeri*, 2 of *L. grayi*, and 69 of *L. monocytogenes* were tested and their scattering patterns were collected. For each species, a representative strain was picked and its analysis is demonstrated here. By comparing the scattering patterns of six cultures of six different species (Fig. 3), each culture could be easily distinguished. The visual analysis of the image revealed unique features; bright center spot, concentric rings, radial spokes, and diffusive spot with various half-angle.

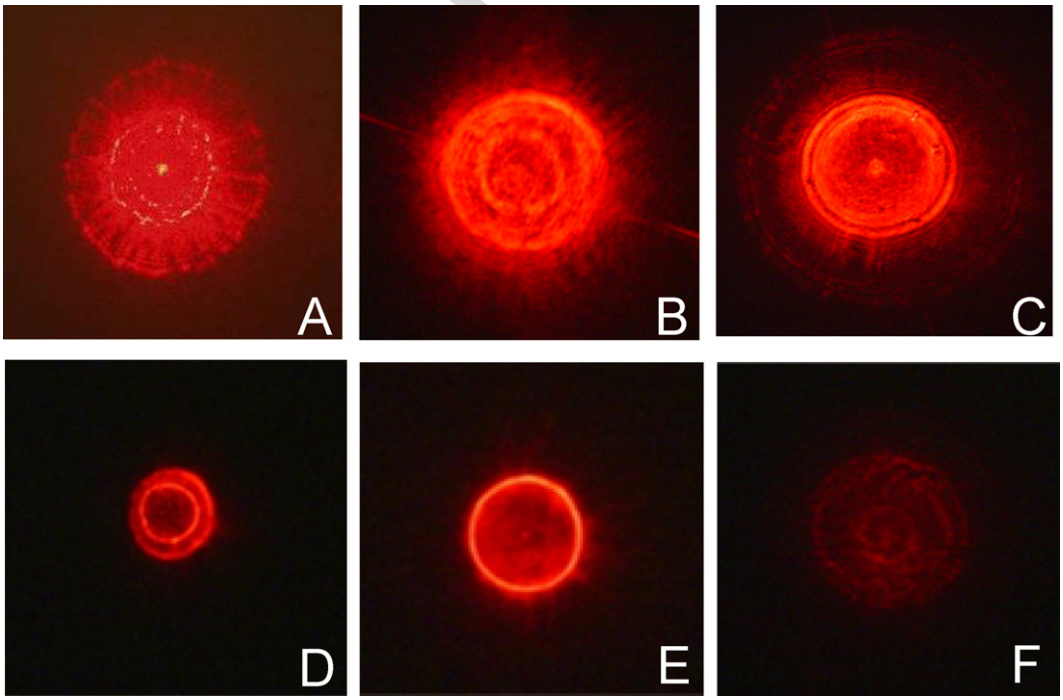

Fig. 3. Scattering-images of representative *Listeria* species: (A) *L. monocytogenes* ATCC19113; (B) *L. ivanovii* ATCC19119; (C) *L. innocua* F4248; (D) *L. seeligeri* LA-15; (E) *L. welshimeri* ATCC35897; (F) *L. grayi* LM37.

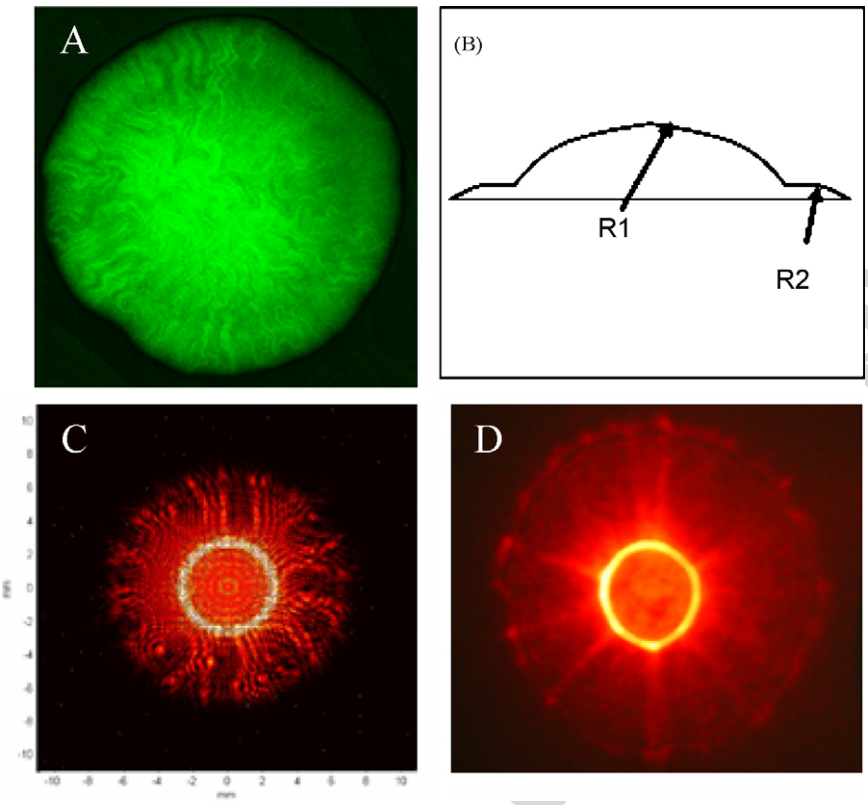

Fig. 4. Comparison of scattering patterns from experiment with simulation: (A) confocal microscopy image of *L. monocytogenes* pNF8 (GFP-producing strain); (B) modeling using two different radii of curvature R_1 and R_2; explaining the two-stage curvature on the colony surface; (C) simulated image with two-stage curvature including radial spoke phase modulation; (D) scattering image for *L. monocytogenes* pNF8 colony.

3.2. Simulation of the forward-scattering pattern using diffraction theory

The biological or microscopic findings were applied in diffraction theory in order to explain the characteristics observed in the scattering patterns. Based on the scattering patterns shown in Fig. 3, the most distinctive characteristics are circular rings, radial spokes and diffuse spots. Physical observation of the colony and optical theory were matched as closely as possible to regenerate the scattering pattern.

L. monocytogenes ATCC 23074 pNF8, a GFP-producing strain was chosen to determine the cross-sectional arrangement of the cells under confocal microscopy, which showed center area and outer annulus with a fuzzy radial feature (Fig. 4A), The one-dimensional orthogonal view of the image also showed core and outer area, which we have modeled with a different effective focal lengths (Fig. 4B). Here we assumed that the edge region was of zero radial extent and that the core region of the colony was a spherical surface with a certain radius of curvature. The colony thickness was about 0.1 mm at the center with a transmission coefficient of $t_1 = 0.8$ for the colony and $t_2 = 0.97$ for the agar area. In this case, the incident beam amplitude distribution was modulated simply by a circular phase object. Comparison of a scattering experiment and a two-dimensional diffraction pattern computed for $z = 300$ mm is demonstrated in Fig. 4C and D. The scattering pattern of *L. monocytogenes* (Fig. 4D) shows a number of ring patterns with a brighter ring in the center region and outward radial spokes. We assumed that the radial spokes are produced by phase modulation with some radial features in the object plane. According to cryo-SEM images (see Supplementary material Fig. 7) there are no microscopic cracks on the surface of the bacterial colony. However, confocal microscopic image of *L. monocytogenes* (Fig. 4A) revealed some kind of obvious radial features. When this type of phase modulation was considered in scalar diffraction theory, radial spokes could be regenerated through diffraction calculation (Fig. 4C). Most of the scattering patterns observed had either a ring or a central spot. The radial spokes were observed only in the species of *L. monocytogenes*.

3.3. Image analysis

We obtained a total of 108 different strains of *Listeria* belonging to six different species (Table 1, see Supplementary material). Our database consisted of 2149 images. Previously, we demonstrated the capability of our system in identifying and grouping *Listeria* species based on their pathogenic potential (Bayraktar et al., 2006). Here, as part of our software development, we tried to effectively group each of the species and to understand the degree of reproducibility and sensitivity of both the scatterometer and the software. Our targeted approach was towards developing a *Listeria* scattering database. As part of our initial analysis, we calculated the feature vectors for 89 images and determined the principal components from these vectors.

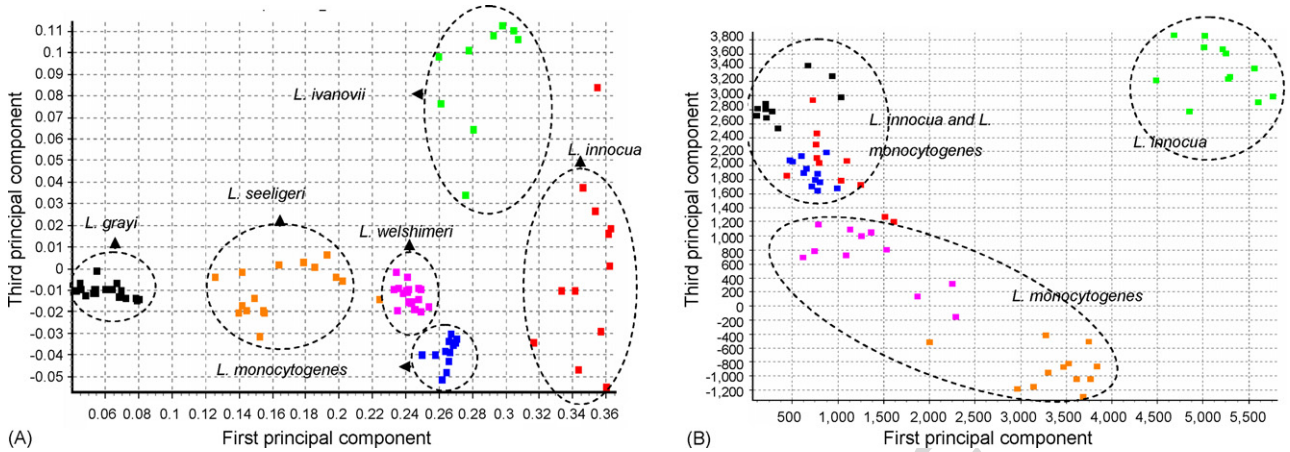

Fig. 5. Principal component analysis (PCA) of forward light-scattering images using cross-products of all Zernike moment invariant features extracted from different *Listeria* spp. (A) and strains of *L. monocytogenes* and *L. innocua* (B). Data for a total of 89 images are shown representing 15–18 images per strain for panel (A). Data for a total of 68 images are shown (panel (B)).

Our feature matrix was 89 × 120 (each column was a specific order Zernike moment and each row was an image and all 120 Zernike moment up to the 20th order-features were used). The first and the third principal components of the images are plotted and different species (and strains) have been marked by different colors (Fig. 5), which are well separated. K-means algorithm gave 100% classification accuracy for *L. ivanovii*, *L. grayi*, *L. welshimeri* and *L. monocytogenes*. The accuracy was 94% for *L. seeligeri* and 91% for *L. innocua*, due to an outlier element (Fig. 5A). Since, *L. monocytogenes* and *L. innocua* are closely related in their genome sequences and cell structure (Lan et al., 2000; Glaser et al., 2001; Buchrieser et al., 2003; Johnson et al., 2004), one of the strains of *L. innocua* (F4248) was grouped distinctively while some strains had overlapping patterns with *L. monocytogenes* (Fig. 5B).

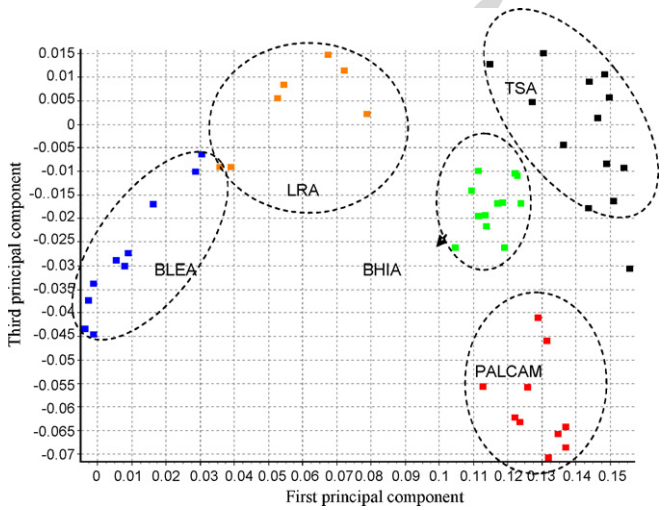

Fig. 6. Principal component analysis (PCA) of forward light-scattering images of *L. monocytogenes* ATCC 19113 grown on different agar surfaces, using covariance of all Zernike moment invariant features. Data for a total of 52 images are shown. TSA: tryptic soy agar; PALCAM: polymyxin B–acriflavin–lithium chloride–ceftazimide–aesculin–mannitol agar; BHIA: brain heart infusion agar; BLEA: buffered *Listeria* enrichment agar; LRA: *Listeria* repair agar.

3.4. Influence of different growth media on the listerial scattering patterns

Changes in the metabolic properties of the bacterial cells lead to changes in the physiological composition of the bacteria and thus the colony. Since our proposition was related to the physiological differences in the colony leading to varied scattering patterns, we demonstrated by growing *L. monocytogenes* ATCC 19113 in different selective and non-selective media. A total of 52 images were used for this analysis (Fig. 6). The well-separated clusters verify our observations that scattering patterns are indeed influenced by growth substrate. The analysis also demonstrates its potential to distinguish small physiological differences.

4. Discussion

Optical scattering technology has been used for identification of bacterial cells in suspension but with limited success due to the problems associated with arrangement of the cells and their orientation (Bronk et al., 2001). To the best of our knowledge, this is the first study where a complete system comprising of a simple light-scattering instrument and efficient identification of bacterial species on a solid nutrient agar surface in conjunction with a reliable and efficient classification tool has been demonstrated.

Our initial exploratory analysis with colonies of *L. monocytogenes*, *L. innocua*, *L. ivanovii*, and *E. coli* provided remarkably distinct scattering patterns (Guo, 2004). Because of the system's undisputed ability to generate such distinct patterns even for closely related *Listeria* species, we decided to concentrate only on *Listeria* and we examined 108 different strains belonging to all the six species. Furthermore, colonies from four cultures were examined by light-scattering method in a blind test and each culture was successfully identified by unaided visual comparison of the scatter images (data not shown).

In order to demonstrate the different features observed in the scattering patterns, we selected one strain of *L. monocytogenes*

as a representative model. Using the confocal image in classical diffraction theory, we could generate simulative models of scattering patterns by changing the radius of curvature. Diffraction theory is a very efficient tool for modeling complex biological images. It has been used to modulate color formation in coronas (Gedzelman and Lock, 2003). The airy ring pattern from a circular aperture is a basic characteristic of diffraction phenomena. It has been considered for plane wave (Hecht, 2002) and Gaussian beam propagation (Nourrit et al., 2001). When millions of bacterial cells form a colony of known size, they form a 'biological aperture' or 'biological lens' with different transmission coefficients for the agar and the colony. However, their physical shape such as radius of curvature deviates severely from perfect lens system, which is still possible to model with phase modulation. In the confocal microscopy image, there are two different distinct areas—circular core and outer annulus. The dimmer rings are caused by the overall circular shape of bacterial colony and the brighter ring in the center believed to be caused by the two different effective focal length which is a function of radii of curvature and refractive index. In addition, we observed a randomly distributed internal structures pointing in outward radial direction which believed to contribute to the scattering as shown in the diffraction calculation. From the diffraction theory, when one-dimensional rectangular aperture is impinged with plane wave, the diffracted wave creates a sin *c* function ($\sin(x)/x$) which is perpendicular to the longitudinal dimension of the rectangular aperture in the object plane (Hecht, 2002). We observed the same kind of sin *c* function intensity modulation in the azimuthal direction since the internal structures were placed in this direction. When this was modeled in the phase modulation part of the integration, we could create radial spokes as in the experimental scattering pattern. A similar effect was reported in the field of telescope optics (Salzman et al., 1982; Richter, 1984) or modulating optical vortices (Curtis and Grier, 2003). However, this application is believed to be the first attempt to apply these functions to biological scattering.

The ultimate goal of this study is to develop a complete system which could be automated with a built-in scatter image database for detection of bacterial colonies growing on semi-solid agar. Therefore, an algorithm was developed where a number of available features were used to adequately represent the patterns in scattering images for distinctive identification. The features are scalar numbers that can be regarded as compact and multiscale object descriptors. Appropriate selection of features for efficient pattern recognition was one of the key factors for the overall success of the process. Features like area, perimeter, and Fourier descriptors (Kim et al., 2002) were too simplistic for the biological images. Therefore, more sophisticated features like Zernike moment invariants were chosen. Moment invariants are scalar values that do not change under affine transformations (when the image is rotated, translated, scaled, and reflected, etc.). Since moments are defined in a continuous domain, moment values are expected to have discretization errors when used in a discrete image domain (Teh and Chin, 1986; Liao and Pawlak, 1998). In our experiments, we chose to use up to the 20th-order Zernike moments in order to include as many characteristics (both coarse and fine) of the patterns as possible. Recombination in which some features were combined into a new one for data reduction was performed using principal component analysis.

In our experiments, there were about 9–20 images per strain, and the original feature vector was made up of 120 Zernike moment invariants. This is a typical example of the 'curse of dimensionality'. Therefore, a stepwise discriminant analysis (SDA) (Huang et al., 2003) would reduce the dimensionality problem from the feature-extraction point of view. Additionally, more features might improve our differentiation capability. New concepts such as Haralick texture features (Haralick et al., 1973; Haralick and Shapiro, 1992) and discrete radial Chebyshev moment invariants (Mukundan et al., 2001; Mukundan, 2004) which have no discretization errors as Zernike moments do, were examined owing to their potential applicability and the results will be published elsewhere.

Thus, the biosensing method developed in the present study is rapid, simple, reagent-less, non-invasive, and sensitive for the identification of bacteria growing on the agar surfaces. It overcomes the problems related to the detection and differentiation of live/dead bacteria which often is a problem with DNA or antibody-based detection systems. The system identifies the bacteria in minutes (5–10 min) compared to the hours (~4–6 h) required by other rapid detection systems.

5. Conclusions

Here, we have demonstrated for the first time, a fast, reliable, non-invasive, sensitive and specific method to differentiate *Listeria* colonies of different species with 91–100% accuracy using a reproducible forward light-scattering scheme and novel image analysis tool. We are currently in the process of acquiring scattering images of several foodborne organisms including *Salmonella enterica*, *E. coli*, *Staphylococcus aureus*, *Enterococcus faecalis*, and species of *Enterobacter*, *Vibrio*, *Aeromonas* and *Bacillus*, which have shown very distinct patterns in our initial steps. We envision the scatterometer will have wide spread application in detection and identification of pathogens not only from food but also from clinical, environment, water, or air samples. The observed high specificity, sensitivity and simplicity of the instrument contribute towards a better identification and classification system.

Acknowledgements

This research was supported through a cooperative agreement with the Agricultural Research Service of the US Department of Agriculture project number 1935-42000-035 and the Center for Food Safety and Engineering at Purdue University. We thank Debby Sherman and Jennifer Sturgis for help with microscopy, Brent Nebeker, Ben Buckner and Amanda Lathrop for technical assistance and consultation.

Appendix A. Supplementary data

Supplementary data associated with this article can be found, in the online version, at doi:10.1016/j.bios.2006.07.028.

References

Bayraktar, B., Banada, P.P., Hirleman, E.D., Bhunia, A.K., Robinson, J.P., Rajwa, B., 2006. J. Biomed. Opt. 11 (3), 034006.

Bhunia, A.K., Lathrop, A., 2003. McGraw-Hill Yearbook of Science and Technology. McGraw-Hill, New York.

Bronk, B.V., Li, Z.Z., Czege, J., 2001. J. Appl. Toxicol. 21, 107–113.

Buchrieser, C., Rusniok, C., Kunst, F., Cossart, P., Glaser, P., 2003. FEMS Immunol. Med. Microbiol. 35, 207–213.

Curtis, J.E., Grier, D.G., 2003. Opt. Lett. 28, 872–874.

Fratamico, P.M., Strobaugh, T.M., Medina, M.B., Gehring, A.G., 1998. Biotechnol. Tech. 12, 571–576.

Gedzelman, S.D., Lock, J.A., 2003. Appl. Opt. 42, 497–504.

Geng, T., Morgan, M.T., Bhunia, A.K., 2004. Appl. Environ. Microbiol. 70, 6138–6146.

Glaser, P., Frangeul, L., Buchrieser, C., Rusniok, C., Amend, A., Baquero, F., Berche, P., Bloecker, H., Brandt, P., Chakraborty, T., Charbit, A., Chetouani, F., Couve, E., de Daruvar, A., Dehoux, P., Domann, E., Dominguez-Bernal, G., Duchaud, E., Durant, L., Dussurget, O., Entian, K.-D., Fsihi, H., Portillo, F.G.-D., Garrido, P., Gautier, L., Goebel, W., Gomez-Lopez, N., Hain, T., Hauf, J., Jackson, D., Jones, L.-M., Kaerst, U., Kreft, J., Kuhn, M., Kunst, F., Kurapkat, G., Madueno, E., Maitournam, A., Vicente, J.M., Ng, E., Nedjari, H., Nordsiek, G., Novella, S., de Pablos, B., Perez-Diaz, J.-C., Purcell, R., Remmel, B., Rose, M., Schlueter, T., Simoes, N., Tierrez, A., Vazquez-Boland, J.-A., Voss, H., Wehland, J., Cossart, P., 2001. Science 294, 849–852.

Goodman, J.W., 1996. Introduction to Fourier Optics, 3rd ed. Roberts & Company Publishers, Greenwood Village, CO.

Guo, S., 2004. Optical scattering for bacterial colony detection and characterization. M.S. Thesis. Purdue University, West Lafayette, IN.

Haralick, R.M., Shanmuga, K., Dinstein, I., 1973. IEEE Trans. Syst. Man Cybern. SMC-3, 610–621.

Haralick, R.M., Shapiro, L.G., 1992. Computer and Robot Vision. Addison-Wesley Publishing Company.

Hecht, E., 2002. Optics. Addison-Wesley, United States.

Hielscher, A.H., Eick, A.A., Mourant, J.R., Shen, D., Freyer, J.P., Bigio, I.J., 1997. Opt. Express 1, 441–453.

Hitchins, A.D., 1998. Food and Drug Administration Bacteriological Analytical Manual, 8th ed. AOAC International, Gaitherburg, MD.

Huang, K., Velliste, M., Murphy, R.F., 2003. SPIE 4962, 298–306.

Hybl, J.D., Lithgow, G.A., Buckley, S.G., 2003. Appl. Spectrosc. 57, 1207–1215.

Ivnitski, D., Abdel-Hamid, I., Atanasov, P., Wilkins, E., 1999. Biosens. Bioelectron. 14, 599–624.

Jaradat, Z.W., Schutze, G.E., Bhunia, A.K., 2002. Int. J. Food Microbiol. 76, 1–10.

Johnson, J., Jinneman, K., Stelma, G., Smith, B.G., Lye, D., Messer, J., Ulaszek, J., Evsen, L., Gendel, S., Bennett, R.W., Swaminathan, B., Pruckler, J., Steigerwalt, A., Kathariou, S., Yildirim, S., Volokhov, D., Rasooly, A., Chizhikov, V., Wiedmann, M., Fortes, E., Duvall, R.E., Hitchins, A.D., 2004. Appl. Environ. Microbiol. 70, 4256–4266.

Kaye, P.H., 1998. Meas. Sci. Technol. 9, 141–149.

Khotanzad, A., Hong, Y.H., 1990. IEEE Trans. Pattern Anal. Mach. Intell. 12, 489–497.

Kim, J.H., Ehrman, S.H., Mulholland, G.W., Germer, T.A., 2002. Appl. Optics 41, 5405–5412.

Lan, Z., Fiedler, F., Kathariou, S., 2000. J. Bacteriol. 182, 6161–6168.

Leidberg, B., Nylander, C., Lundstrom, I., 1983. Sens. Actuators B: Chem. 4, 299–304.

Liao, S.X., Pawlak, M., 1998. IEEE Trans. Pattern Anal. Mach. Intell. 20, 1358–1364.

Ligler, F.S., Taitt, C.R., Shiver-Lake, L.C., Sapsford, K.E., Shubin, Y., Golden, J.P., 2003. Anal. Bioanal. Chem. 377, 469–477.

Mukundan, R., 2004. Proceedings of the Sixth IASTED Conference on Signal and Image Processing (SIP2004) Honolulu, pp. 80–84.

Mukundan, R., Ong, S.H., Lee, P.A., 2001. International Conference on Imaging Science Systems and Technology (CISST'01) Las Vegas, pp. 23–29.

Nebeker, B.M., Buckner, B., Hirleman, E.D., Lathrop, A., Bhunia, A.K., 2001. Proc. SPIE 4206, 224–234.

Nourrit, V., de Bougrenet de la Tocnaye, J.-L., Chanclou, P., 2001. J. Opt. Soc. Am. A 18, 546–556.

Perkins, E.A., Squirrell, D.J., 2000. Biosens. Bioelectron. 14, 853–859.

Richter, J.L., 1984. Appl. Optics 23, 1907–1913.

Salzman, G.C., Griffith, J.K., Gregg, C.T., 1982. Appl. Environ. Microbiol. 44, 1081–1085.

Scully, M.O., Kattawar, G.W., Lucht, R.P., Opatrný, T., Pilloff, H., Rebane, A., Sokolov, A.V., Zubairy, M.S., 2002. Proc. Natl. Acad. Sci. U.S.A. 99, 10994–11001.

Shapiro, H.M., 2003. Practical Flow Cytometry, 4th ed. Wiley-Liss, Hoboken, NJ.

Stull, V.R., 1972. J. Bacteriol. 109, 1301–1303.

Teh, C.H., Chin, R.T., 1986. Comp. Vision Graphics Image Proc. 33, 318–326.

Vazquez-Boland, J.-A., Kuhn, M., Berche, P., Chakraborty, T., Dominguez-Bernal, G., Goebel, W., Gonzalez-Zorn, B., Wehland, J., Kreft, J., 2001. Clin. Microbiol. Rev. 14, 584–640.

Warner, T.L., Hirleman, E.D., 1997. J. Inst. Environ. Sci. 40, 15–21.

Wyatt, P.J., 1969. Nature 221, 1257–1258.

Wyatt, P.J., Phillips, D.T., 1972. J. Theor. Biol. 37, 493–501.